COBEM 2023 27TH INTERNATIONAL CONGRESS OF MECHANICAL ENGENEERING

ABCM Brazilian Society of Mechanical Sciences and Engineering
27th ABCM International Congress of Mechanical Engineering
December 04-08, 2023, Florianópolis-SC, Brazil

COB-2023-2271
EXPERIMENTAL INVESTIGATION OF THE BOUNDARY LAYER TRANSITION OVER SURFACE IRREGULARITIES

Rafael Estorniolo
Felipe Oliveira Aguirre
Victor Barcelos Victorino
Marcello Augusto Faraco de Medeiros
University of São Paulo, São Carlos, São Paulo, 13563-120, Brazil;
rafael.estorniolo@usp.br
felipe.aguirre@usp.br
barcelos.victorino@usp.br
marcello@sc.usp.br

Abstract. *Nowadays, with an ever-growing focus on environmental sustainability and cost-effectiveness, it has become essential to comprehend the impact of surface irregularities on the boundary layer transition. This is particularly important when considering the rise in friction drag due to turbulent boundary layers, which can significantly impact the performance and efficiency of aerodynamic surfaces. Thus, this paper presents an experimental investigation that aims to shed light on the differences in the boundary layer transition process induced by bumps and gaps. By comparing the natural and bypass transition processes, using hot-wire anemometry and a Preston tube, this study provides insights into the behavior of flow over surface irregularities. The experiments were conducted in the low acoustic noise and turbulence wind tunnel of the University of São Paulo (LANT - EESC/USP). The model employed is a flat plate with a chord of 2.32 m and an insert that forms the gap and the bump. The findings of this study have implications for the design of aerodynamic surfaces. Therefore, this study contributes to the development of more efficient and sustainable solutions for various engineering applications, making it a crucial step forward in the field of aerodynamics.*

Keywords: *Boundary Layer Transition, Surface Irregularities, Bumps, Gaps*

1. INTRODUCTION

Viscous drag is responsible for reducing aerodynamic efficiency and, consequently, bringing several unwanted effects, such as an increase in an aircraft's fuel consumption, higher emissions of harmful gases, and higher levels of aeroacoustic noise, among others. Reneaux (2004) estimated that about 22% of the operating costs of an aircraft were related to fuel consumption, at a time when the average price of a barrel of oil was 40 dollars. Today, the price has practically doubled. One of the factors responsible for the increase in viscous drag is the turbulent boundary layer, which usually becomes turbulent after the growth of unstable modes that leads to the transition. In two-dimensional boundary layers, the growth of Tollmien-Schlichting (TS) waves is the mechanism that leads to natural transition, as experimentally demonstrated by Schubauer and Skramstad (1947). Additionally, TS waves can interact with geometric imperfections present on the surface, as shown by Crouch (2006). These irregularities can be steps, bumps, gaps, and others. Crouch and Kosorygin (2020) distinguished steps, bumps and gaps geometrically in their work. In fact, these irregularities are observed on the surface of real aircraft, such as rivets, plate edges, dirt, paint delamination, etc. On the other hand, depending on the geometry and/or flow conditions, these imperfections can bypass the growth of TS waves, as observed by Beguet *et al.* (2017) and Crouch *et al.* (2022). In other words, another mechanism, as described by Saric *et al.* (2002), rather than the TS waves causes the boundary layer transition.

The effect of surface irregularities has drawn the attention of researchers since the last century. Tani *et al.* (1940) experimentally investigated the effect of a round transversal wire resting over a flat plate on the boundary layer transition. The authors studied the parametric dependence of the wire diameter on the transition Reynolds number. Regarding forward-facing steps, the work by Stuper (1949) employed a similar analysis. A review on this topic was reported by Dryden (1949). These experiments showed the influence of the roughness size on the transition Reynolds, which decreases. In other words, the transition location moves upstream towards the imperfection. Later, Klebanoff and Tidstrom (1972) indicated that the recovery zone, which is the region immediately downstream of the imperfection (transversal cylindrical rod), presents a distortion of the mean flow, causing a destabilizing effect on the boundary layer. Cebeci and Egan (1989) developed a combination of an interactive procedure and the semi-empirical e^N method from Smith *et al.* (1956) and van Ingen (1956) to predict the transition location due to a bump. The authors pointed out that the bump influences the critical frequency, which is the first-dimensional frequency that reaches an integral growth beyond the transition threshold.

Nayfeh *et al.* (1988) performed a similar study and also concluded that the bump tends to alter the frequency that leads to transition compared to the smooth case. Furthermore, they found that the bump height and its streamwise location are the key parameters of the instability, and also that the separation bubble size downstream of the obstacle impacts on the transition location. According to Masad and Iyer (1994), this separation bubble provokes a considerable change in the transition point. They also reported that for bump heights larger than a determined value, which is larger than the bump height that causes separation, the transition occurs abruptly over the bump. Concerning steps, Wang and Gaster (2005) built an empirical tool using experimental data that relates to the e^N method. The relation between the position of the transition and h/δ^* can be divided into 3 regions: (i) the presence of the step does not interfere in the transition, (ii) a curve where the transition approaches the step, and (iii) a saturation value of h/δ^* which the transition takes place in the step itself.

The effect of gaps is similar to the other imperfections. Some of the first experimental studies were conducted by Sarohia (1977) and Sinha *et al.* (1982). Sinha *et al.* (1982) analyzed the effect of parameters such as the depth and width of the gaps, classifying them as shallow or deep, open or closed, however, their results did not indicate anything about the effects on the transition point. Sarohia (1977) determined the limits in which the cavity causes oscillatory motion. The results from several flow conditions collapsed in one curve according to the non-dimensional parameter $(L/\delta)\sqrt{Re_\delta}$. Although his study did not address the impact of the cavity on the transition, the cavity oscillation limits resemble the bypass transition limits later investigated by Beguet *et al.* (2017) and Crouch *et al.* (2022). Regarding the impact of gaps in the transition, Beguet *et al.* (2017) established an empirical relationship that relates depth (D), length (L) and displacement thickness (δ^*) with the N factor. According to the authors, the behaviour of the N factor can be subdivided into two: a peak of amplification over the gap (N_{peak}) that decays to a shifted up curve parallel to the amplification from the smooth case (N_{far}). Moreover, they reported the so-called tripping limits, i.e. values of $L/\delta^* \geq 18$ and $D/\delta^* \geq 2$ where the transition occurs over the gap. Crouch *et al.* (2022) also found a similar bound and they considered this behavior due to bypass transition, not to mention a high-frequency oscillation, very different from the TS range, measured in a particular case in the bypass transition region. Furthermore, they experimentally modeled the impact of gaps on the transition depending on depth and length. They proposed an equation to estimate the transition location change in terms of ΔN as a function of the gap length and the aspect ratio. The latter parameter is related to the plateau where ΔN remains constant as L/δ^* is increased. The authors refer to this as a deep-gap limiting case. Victorino *et al.* (2023) computationally found a connection between this bypass transition and unstable modes in the cavity, such as Rossiter and centrifugal modes. In this study, the linear stability analysis indicates that the centrifugal mode neutrality is lower than the Rossiter's, which takes place near the bypass transition bounds from Crouch *et al.* (2022) and Beguet *et al.* (2017). The linear stability analysis of one particular case (case C) presented an unstable Rossiter mode with frequency 4% different from the experimentally measured by Crouch *et al.* (2022). Moreover, the DNS exhibited a non-linear interaction between the centrifugal and Rossiter modes leading to transition.

This paper compares the evolution of velocity disturbances and boundary layer transition induced by different configurations of bumps and gaps in regimes dominated by TS waves and bypass transition. The stream-wise evolution of the fluctuation velocity signals is analyzed in both time and spectral domain and is compared to the linear stability theory. Aside from this, gaps and bumps with the same depths/heights are compared. Studying the different transition mechanisms involved in this problem may aid in comprehending the physics, the phenomena that take place, and the regimes. As a result, more accurate models to predict the transition location can be developed, and better passive control of laminar-turbulent transition can be reached, promoting better aerodynamic performance and more sustainable aircraft.

2. METHODOLOGY

The experiments were performed at LANT (Low Acoustic Noise and Turbulence), a closed-circuit wind tunnel at EESC-USP. It has a square test section with dimensions 1 m $\times$ 1 m and a length of 3 m. More details about the wind tunnel are available at Amaral *et al.* (2021). As the name suggests, it features low acoustic noise and turbulence level in the free-stream, with a value of $Tu = 0.038\%$ (bandwidth 1-1024 Hz) measured with the empty test section and free-stream of 20 m/s. The turbulent intensity measured with the model installed in the test section was $Tu = 0.054\%$ (bandwidth 4-1024 Hz) at 27 m/s. In addition, it presents good levels of uniformity, with velocity variations of the order of 1% of free-stream in an area of 600 mm $\times$ 600 mm in the center of the test section.

The test model used is a flat aluminum plate, with dimensions of 2320 mm $\times$ 1000 mm $\times$ 10 mm. It presents a tab and a flap, for adjusting the pressure gradient, which for a Blasius profile should be as zero as possible. The CAD section view of the model is shown in Fig. 1. The plate has an insert that houses a system that changes the geometry of the surface imperfection, i.e. it is possible to form a smooth flat plate, a bump or a gap. This system is positioned 600 mm from the leading edge of the model. The bump has dimensions of 30 mm in length in the flow direction and a span of 600 mm. The span is significantly larger than the other dimensions to avoid edge effects on the central line of the model. The bump height, or gap depth, has a stroke of 20 mm and is driven by two stepper motors installed at the bottom of this part. The maximum resolution of gap/bump movement is 20 μm.

The instrumentation used in the present study will be presented. The velocity, both average and fluctuation, was

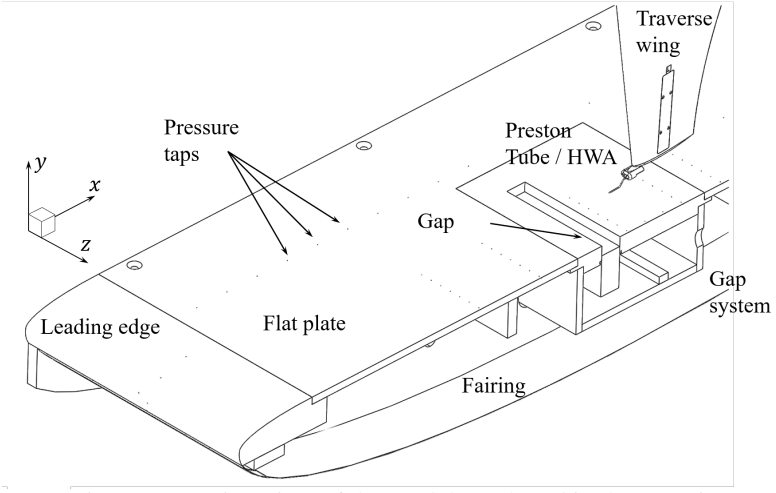

Figure 1: Section view of the model employed in the experiments

measured using Hot Wire Anemometry (HWA). The anemometer used is AN-1002 from the A.A.Lab system, operating in CTA (Constant Temperature Anemometry) mode. The probe used as a sensitive element is the Dantec Dynamic model 55P15, indicated for boundary layer measurements. The probe can be moved to the desired point using a high-precision 3D Cartesian traverse, with a movement resolution in the normal direction to the wall (y) of 6.25 μm. A wing covers the traverse rod to prevent vortex shedding and, consequently, unwanted vibrations that can contaminate the fluctuating velocity signal. This wing also houses other sensors, such as the Preston tube and the LVDT distance sensor, used to measure the distance between the sensors and the plate. The anemometer output signal is sent to two data acquisition modules. The former, DAq-USB-6002 from National Instruments, is used for average velocity measurements and features 16-bit resolution and a sampling rate of up to 50,000 samples per second. The anemometer voltage values are converted into velocity through calibration with velocity values measured by a static Pitot positioned inside the test section. The latter consists of a PXI-4496 board with 24-bit resolution installed in a PXI-1042Q chassis, both from National Instruments and due to its higher resolution, it is responsible for acquiring the voltage fluctuation signal. Finally, the Preston tube is used to estimate the transition location. This instrument measures the dynamic pressure of the flow over the wall. Therefore, when a transition occurs, the derivative of the velocity profile changes and, as a consequence, the dynamic pressure measured by the instrument increases abruptly. Thus, the minimum Preston tube value indicates the transition location. The total pressure sensing element consists of a needle with a diameter of 0.9 mm carefully bent in a similar shape to the hot-wire probe. On the other hand, the static pressure of the free-stream is measured through a Pitot located on the wing of the traverse. A Honeywell RSC differential pressure transducer is employed to acquire the pressure data, presenting a total error of less than 5 Pa.

The experiment consisted of two different types of measurements: (i) a Preston tube sweep along the streamwise direction to detect the transition location and (ii) hot-wire fluctuation velocity records at specific positions to characterize the disturbance evolution along the streamwise axis. Both types of measurements were performed simultaneously. Additionally, at each x position the irregularity height was changed accordingly to the predefined values: $h = 0$, ± 0.8, ± 1.6, and ± 4 mm. From herein we establish that $h > 0$ is a bump, whereas $h < 0$ is a gap. The free-stream velocity was kept constant at $U_\infty = 20$ m/s. The experimental grid was different and adapted to each type of measurement. The Preston tube measurement stations presented two different spacing, 10 mm in the range $640 \leq x \leq 700$ mm and a larger spacing of 50 mm in the remaining extent of the model up to $x = 1900$ mm. In this manner, it was possible to verify the occurrence of an eventual backflow region near downstream of the bump as reported by Klebanoff and Tidstrom (1972); Nayfeh *et al.* (1988); Masad and Iyer (1994). To characterize the disturbances we measured hot-wire signals at $x = 640$ mm, capturing the near-field influence of the irregularity, and the far-field evolution in the range $700 \leq x \leq 1900$ mm with spacing of 100 mm. Concerning the wall-normal distance, we positioned the hot-wire probe at a constant non-dimensional distance ($\eta = y\sqrt{\nu x/U_\infty} \approx 1.23$) where the Blasius velocity profile presents $U/U_\infty = 0.4$, which corresponds to the region where the TS maximum amplitude occurs.

3. RESULTS

Table 1 condenses information regarding the surface irregularity, the transition location determined by the Preston tube, and the transition mechanism, which will be further discussed. For the free-stream velocity employed, the transition in the smooth case was not reached, as in one case with a gap, because the flat plate's length was not sufficient to reach the transition Reynolds number. Another experiment with higher velocity showed that the transition Reynolds number for the smooth flat plate occurs at $Re_x = 2.4(10^6)$. However, the transition occurred in the cases G2, G3, B1, B2, and

Table 1: Cases covered and their respective transition location and mechanism.

Case	Irregularity	h/δ^*	Transition x [m]	$Re_x(10^6)$	Transition Mechanism
G3	Gap	-3.22	0.64	0.74	Bypass
G2	Gap	-1.29	1.90	1.28	TS
G1	Gap	-0.64	-	-	TS
S	Smooth	0	-	-	TS
B1	Bump	0.64	1.60	1.86	TS
B2	Bump	1.29	0.70	0.82	TS or Bypass
B3	Bump	3.22	0.64	0.74	Bypass

B3. Such a result indicates that for a constant Re_{δ^*} a bump is more destabilizing than a gap with the same height relative to the displacement thickness. A comparison between the transition Re_x and the semi-empirical model by Wang and Gaster (2005) regarding backward-facing steps presented a reasonable agreement. The transition Reynolds numbers of the case B1 and B2 were $Re_x = 1.86(10^6)$ and $0.82(10^6)$, respectively, whereas the extracted from the curve by Wang and Gaster (2005) for the same backward-facing step height were $Re_x = 1.86(10^6)$ and $1.01(10^6)$. It is expected that the impact of a bump with a higher aspect ratio L/h resembles the one from a backward-facing step. Therefore, this fact helps explain why the case B1 ($L/h = 37.5$) presented a better agreement than the case B2 ($L/h = 18.75$). Moreover, Crouch and Kosorygin (2020) suggests that the impact on the transition Reynolds number for a bump is a combination of a forward-facing and a backward-facing step. Since the impact of a forward-facing step with $h/\delta^* = 0.64$ is negligible according to Wang and Gaster (2005), but more prominent for $h/\delta^* = 1.29$, this also supports that bumps with relative height $h/\delta^* < 1$ influence the transition similarly to a backward-facing step.

3.1 Transition dominated by TS instability

Next, we present the stream-wise evolution of the fluctuation velocity. The signals were analyzed in both the time and frequency domain. For the frequency domain analysis, we employed Welch's method that computes the power spectral density (PSD) by taking the ensemble average of PSD from 90 smaller segments of the original time series with 50% overlap (179 ensembles). In this manner, it is possible to increase the signal-to-noise ratio by reducing the frequency resolution as a trade-off. Moreover, a Hanning window function was applied in each segment to attenuate side-lobe leakage, and the scale factor of $\sqrt{(8/3)}$ was applied to correct the magnitudes according to Bendat and Piersol (2010). Once the ensemble-averaged PSD was computed, the amplitude of each frequency component could easily be calculated by taking its square root. As a high-frequency Rossiter mode can develop, a sampling rate of 10000 samples/s was employed. Figure 2 exhibits the stream-wise evolution of the spectra for cases S, G1, B1, G2, and B2. Similarly, Fig. 3 depicts the contours of the amplitudes with respect to the non-dimensional axes Re_{δ^*} and $2\pi f\nu/U^2(10^6)$ compared to the theoretical unstable diagram from the solution of the Orr-Sommerfeld Equation. The smooth case (S) is placed in the central row of each figure to aid the comparison, whereas each column represents gap and bump, respectively. We can break down the spectra into two regions: a low-frequency range ($f \leq 50Hz$) with high amplitude and the remaining frequency range. Although the low-frequency range presents a great portion of the oscillatory energy, it does not evolve with respect to the streamwise axis except when turbulence occurs. Literature refers to this range as a wind tunnel's background noise according to Wang and Gaster (2005). The spectra also present some sharp peaks related to electrical noise, however, it does not affect the interpretation of the results.

Firstly analysing the smooth case (S), we can see that a band of frequencies with a shape similar to a bell amplifies with respect to the streamwise axis. This band corresponds to the TS unstable frequency band, as shown in Fig. 3. As predicted by the theory, the dimensional frequency band changes with respect to Re_{δ^*} (x), moving from higher frequencies ($200 \leq f[Hz] \leq 400$) in the most upstream position to lower frequencies ($70 \leq f[Hz] \leq 200$) in the most downstream position. Next, for the pair of gap and bump with height $|h/\delta^*| = 0.64$, we can see that the spectrum evolution is very different from each other. In the station most upstream ($x = 0.64$ m), the gap (G1) affects most prominently the TS band. However, the bump (B1) presents larger amplitudes at lower and mid frequencies (10-600 Hz). Furthermore, a high-frequency bulge centered around 900 Hz emerges in the spectrum. Seemingly, the bump locally promotes an adverse pressure gradient near its trailing edge, displacing branch II of the stability region in a manner that favors the amplification of higher frequencies at this Reynolds number. The Preston tube readings corroborate this hypothesis since they indicate lower values of dynamic pressure at the wall, compared to the smooth case at the same position, which can be caused by a velocity profile typical of an adverse pressure gradient. Finally, the cases G2 and B2 present more drastic differences between each other. Concerning the case G2, the spectrum at the gap's near-field is practically flat and presents larger amplitudes. Further downstream, these high amplitude oscillations spatially decay in an abrupt form. These indicate that the flow past the gap presents oscillatory motion which is not sustained downstream in the boundary layer, most likely

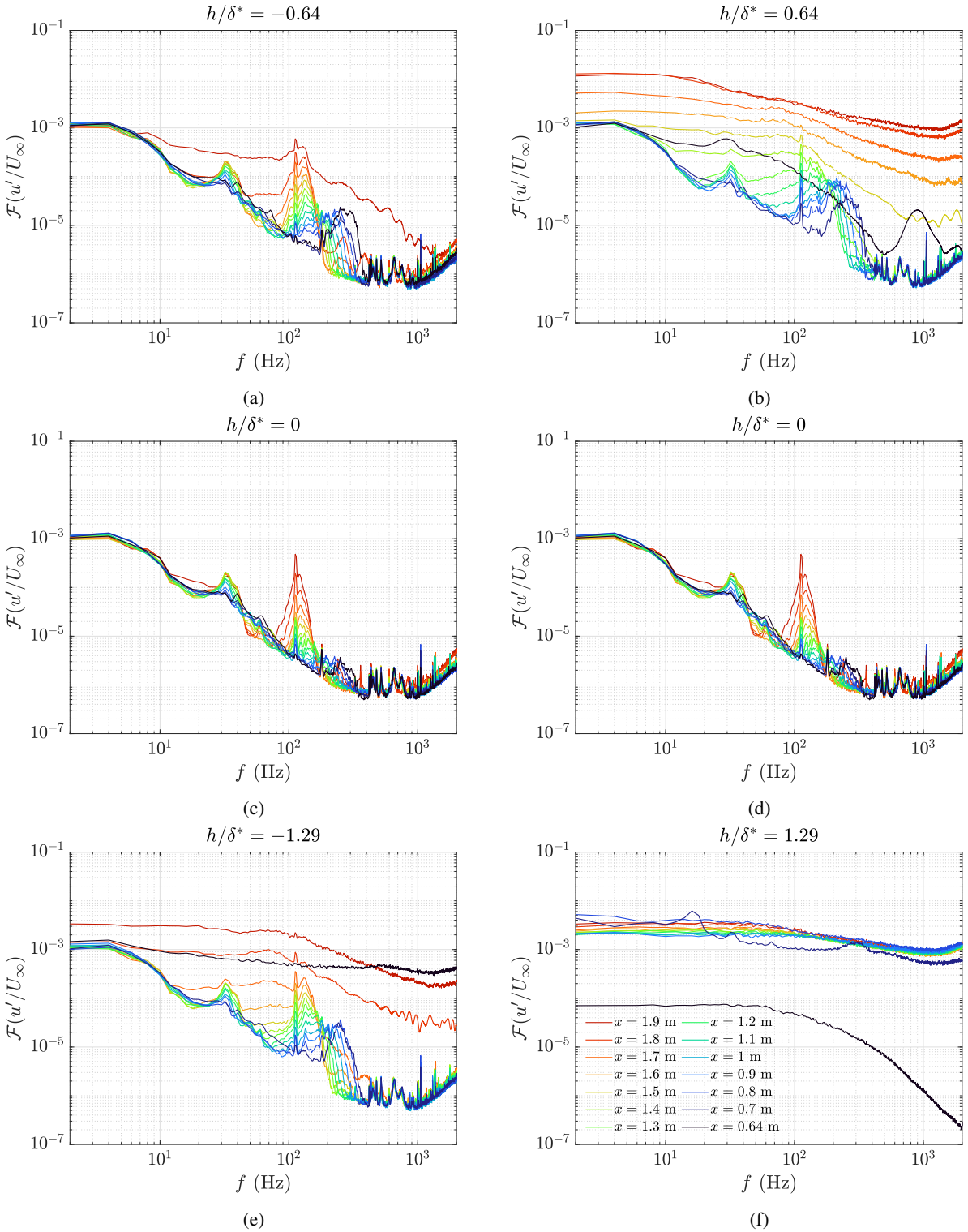

Figure 2: Amplitude of the signals collected by HWA in different configurations of irregularities

because does not comprise the unstable TS range. However, the TS band is excited by the gap and this can be visualized by energy spread out within the unstable region as exhibited in Fig. 3e. As a consequence, the TS amplitude is larger compared to the smooth case, the reason why the transition occurred at $x = 1.9$ m in the case G2, but did not occur in the smooth case (S). On the other hand, case B2 revealed a strong destabilization of the boundary layer caused by the bump leading to an abrupt transition. Since few measurements were collected in the region, it is unclear whether the transition mechanism occurred due to the growth of TS waves or bypassed by another mechanism.

To quantify the amplitude growth, the N-factor was estimated in the configurations $h/\delta^* = \pm 0.64$ (B1 and G1 cases) as $\ln(A/A_0)$ using the amplitude of the dominant frequency observed in the most downstream x position of the smooth case.

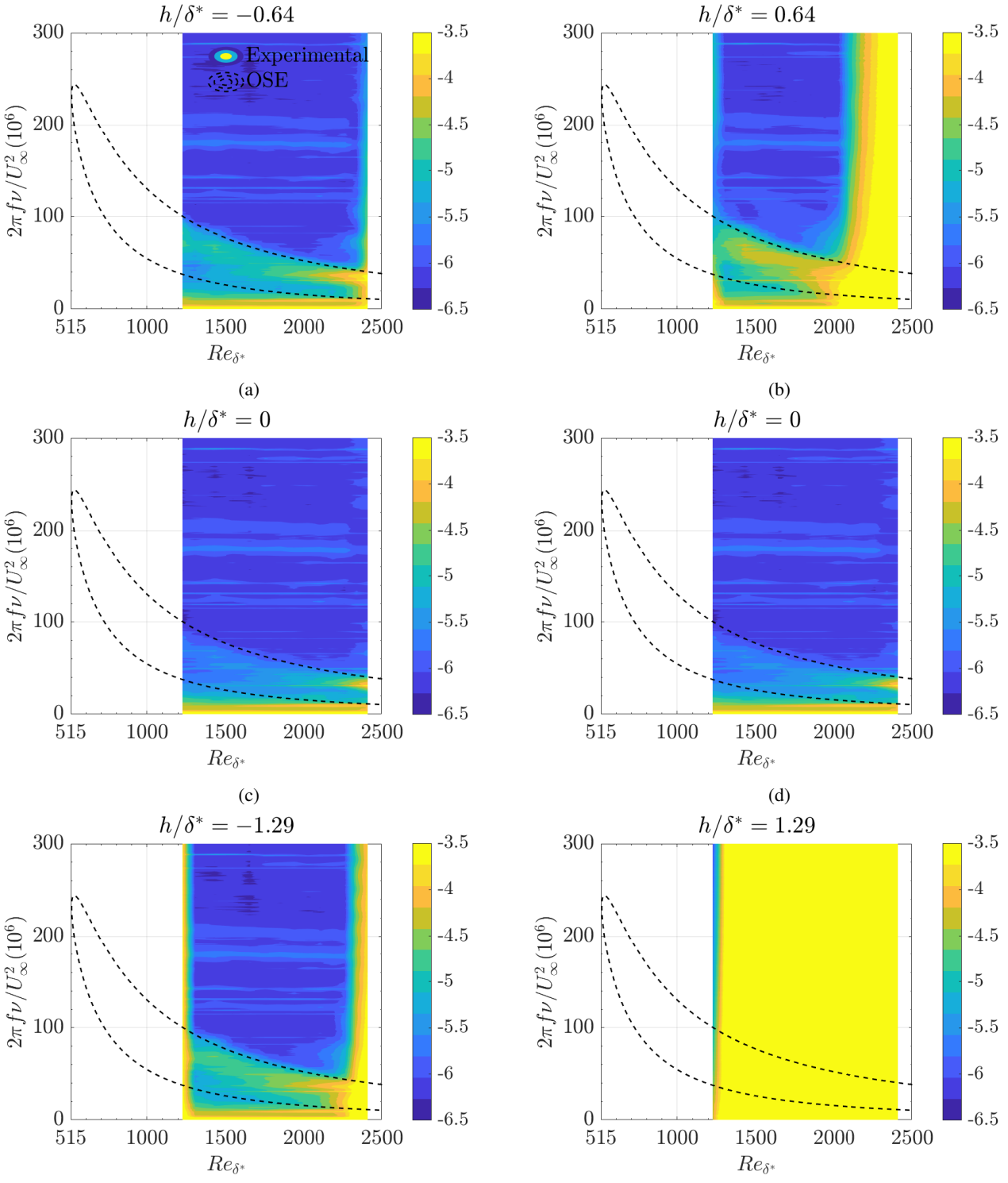

Figure 3: Amplified frequency band in each irregularity configuration compared to the Orr-Sommerfeld equation

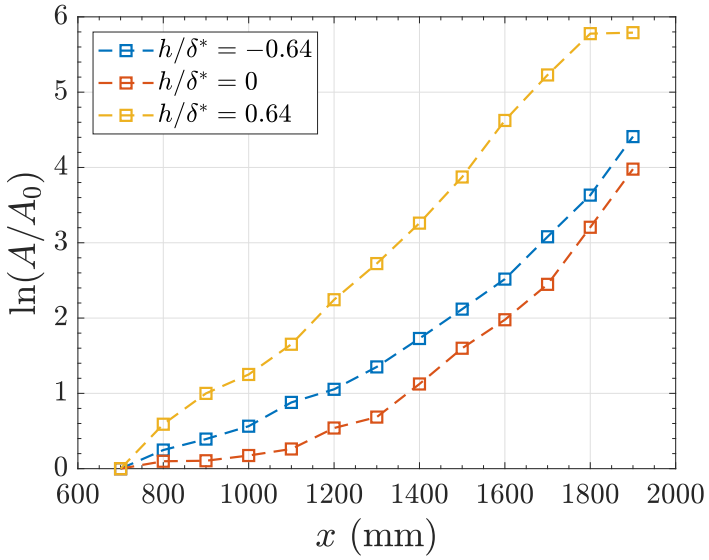

Figure 4: Amplitude ratio between the smooth case, the bump with $h/\delta^* = 0.64$ and the gap with $h/\delta^* = -0.64$.

Figure 4 displays the N factor along the streamwise direction of the cases B1, S and G1. The bump indeed causes more amplification than the gap. The ΔNs between each configuration and the smooth case estimated were: $\Delta N_{Bump} = 2.6$ and $\Delta N_{Gap} = 0.4$.

3.2 Bypass transition regime

Cases B3 and G3 both presented bypass transition, each one with its particularities. Figure 5 shows the streamwise evolution of the fluctuation velocity spectrum of the case G3, acquired similarly as previously presented. It is possible to observe a sharp peak in the fluctuation velocity spectrum with a relatively larger amplitude and higher frequency when compared to the TS band from the smooth flat plate case in a similar streamwise position. This peak is attributed to the Rossiter mode. The non-dimensional frequency was $fL/U = 0.78$ and is close to the Rossiter second mode (R_2) according to Rossiter (1966) and Block (1976) formulas. The Rossiter mode amplitude spatially decays downstream of the gap, since it excites a TS frequency which is stable according to the linear stability theory for the local Reynolds number. Moreover, the spectra show turbulence characteristics and the low-frequency magnitudes tend to amplify along the streamwise axis due to the turbulence development. Although the centrifugal mode was not identified in the spectra, this experimental evidence supports the numerical study by Victorino *et al.* (2023), in which the combination of centrifugal and Rossiter modes triggered the transition.

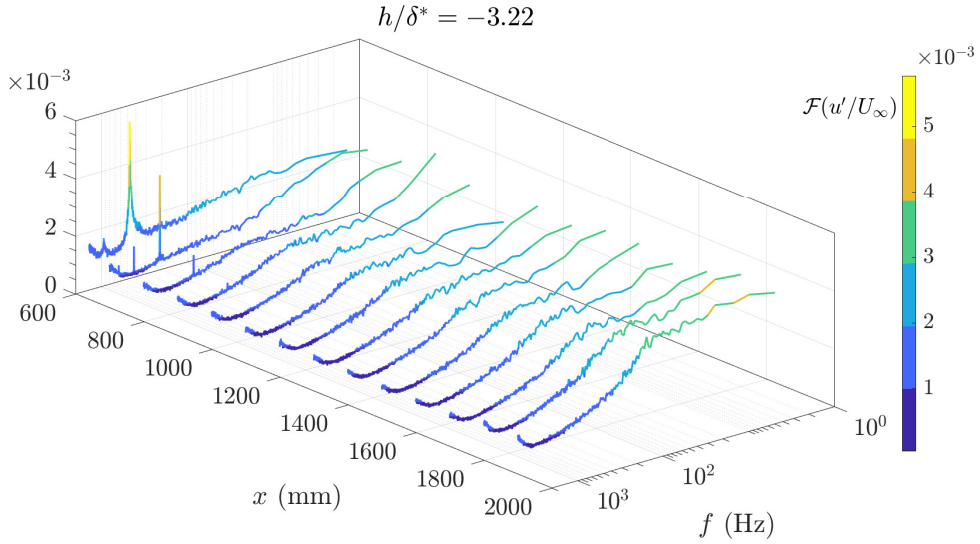

Figure 5: Disturbance velocity evolution along the streamwise direction of the spectrum of the G3 gap case ($h/\delta^* = -3, 22$) exhibiting the presence of the Rossiter mode near the gap.

Figure 6 shows Preston tube data for cases G3, S and B3. As previously discussed, G3 is already turbulent immediately downstream of the gap. We can see that the dynamic pressure at the wall measured by the Preston tube has a trend similar to the smooth case, however, at a higher level. In opposition, case B3 dynamic pressure at the wall has a different behavior immediately downstream of the bump. It suddenly grows from a negative value to levels equivalent to the dynamic pressure from the case G3 which has a turbulent boundary layer. This negative dynamic pressure region suggests the presence of a velocity profile with reverse flow caused by a separation bubble located downstream of the trailing edge of the bump. This result agrees with the reported by Nayfeh *et al.* (1988) and Masad and Iyer (1994) which state that the presence of this separation bubble provokes a big impact on the transition process.

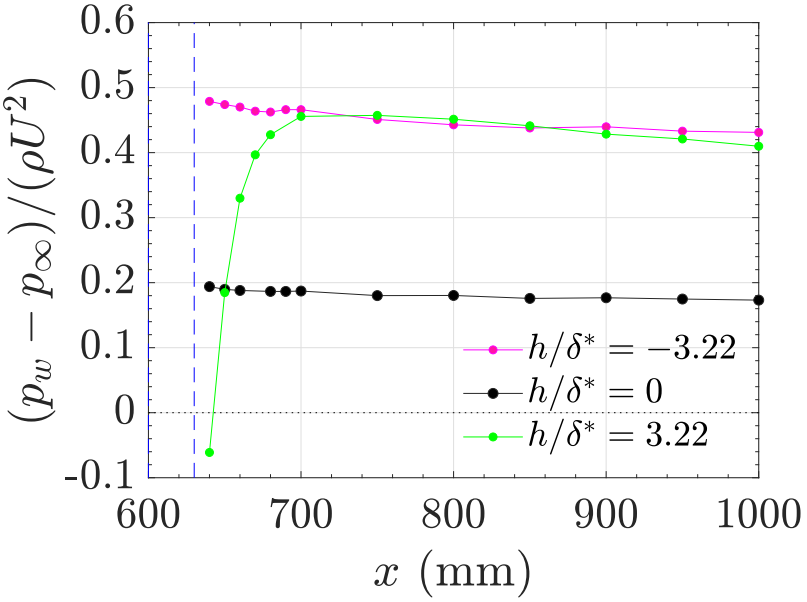

Figure 6: Preston tube data evidencing a backflow region (re-circulation bubble)

4. CONCLUSION

This paper addresses the experimental investigation of the stability and transition of a boundary layer containing an interchangeable surface irregularity that can form a bump or a gap. To characterize the transition process and also to quantify the impact on the TS growth due to the surface irregularities, HWA and Preston tube data were analyzed.

Firstly, a good agreement between the experimental data and theoretical results was achieved, indicating that indeed the TS unstable frequencies matched the predicted by the theory.

Secondly, we compared bumps and gaps with the same height relative to the local displacement thickness and Reynolds number. The results indicated that bumps provoke a higher impact on the TS growth than the gap, causing a larger shift of the transition location towards the surface irregularity. This was visible when comparing the disturbance amplitude growth and quantified through the ΔN.

Thirdly, the bypass transition from each type of irregularity was studied. Concerning the gap, we observed the Rossiter instability with a frequency close to the second mode R_2 predicted by the semi-empirical formulas by Rossiter (1966) and Block (1976). Additionally, the experiments corroborated the numerical study from Victorino *et al.* (2023), in which the Rossiter mode appeared as the transition mechanism. Regarding the bump, the critical height that causes the bypass transition appeared to be lower than the critical depth of a gap. Preston tube data revealed a separation bubble attached to the bump's leading edge, indicating that the bubble plays a role in the bypass transition in bumps. Such a result was also observed by Nayfeh *et al.* (1988) and Masad and Iyer (1994).

Therefore, we conclude that in the case of surface roughness with similar dimensions, bumps contribute more to boundary layer instability and transition than gaps. Thus, in the case of manufacturing aerodynamic surfaces that require high efficiency, i.e. as little drag as possible, it is preferable to opt for the presence of gaps rather than bumps.

5. ACKNOWLEDGEMENTS

R.E. thanks the National Council for Scientific and Technological Development (CNPq) for the undergraduate research scholarship (PIBIC). F.O.A. and V.B.V. would like to thank the Coordination of Superior Level Staff Improvement (CAPES) for the PhD's scholarships. M.A.F.M. thanks the National Council for Scientific and Technological Development (CNPq) grant no. 307956/2019-9, the Agency for Financing Studies and Projects (FINEP) grant no. 01.09.0334.04,

The Sao Paulo Research Foundation (FAPESP) grant no. 2019/15366-7, The Boeing Company grant no. 2021-GT-353, and the US Air Force Office of Scientific Research (AFOSR) for grants FA9550-18-1-0112, managed by Dr. Geoffrey Andersen under supervision by Lt. Col. Daniel Montes from SOARD, and FA9550-23-1-0030, managed by Dr. Roger Greenwood.

6. REFERENCES

Amaral, F.R., Rico, J.C.S., Bresci, C.S., Beraldo, M.M., Victorino, V.B., Gennaro, E.M. and Medeiros, M.A.F., 2021. "The low acoustic noise and turbulence wind tunnel of the university of sao paulo". *The Aeronautical Journal*, pp. 1–45.

Beguet, S., Perraud, J., Forte, M. and Brazier, J.P., 2017. "Modeling of transverse gaps effects on boundary-layer transition". *JOURNAL OF AIRCRAFT*, Vol. 54, p. 794–801.

Bendat, J.S. and Piersol, A., 2010. *Random Data, Anaysis and Measurement Procedures*. John Wiley and Sons, New York.

Block, P.J.W., 1976. "Noise response of cavities of varying dimensions at subsonic speeds". Technical Report TN D-8351, National Aeronautics and Space Administration.

Cebeci, T. and Egan, D.A., 1989. "Prediction of transition due to isolated roughness". *AIAA Journal*, Vol. 27, No. 7, pp. 870–875.

Crouch, J.D., 2006. "Instabilities in boundary-layer flows and their role in engineering". *IUTAM Symposium on One Hundred Years of Boundary Layer Research*, p. 105–114.

Crouch, J.D. and Kosorygin, V.S., 2020. "Surface step effects on boundary-layer transition dominated by tollmien–schlichting instability". *AIAA Journal*, Vol. 58, No. 7, pp. 2943–2950.

Crouch, J.D., V. S. Kosorygin, M.I.S. and Miller, G.D., 2022. "Characterizing surface-gap effects on boundary-layer transition dominated by tollmien–schlichting instability". *Flow*, pp. 1–14.

Dryden, H.L., 1949. "Review of published data on the effect of roughness on transition from laminar to turbulent flow". *National Advisory Committee for Aeronautics*, pp. 477–482.

Klebanoff, P.S. and Tidstrom, K.D., 1972. "Mechanism by which a twodimensional roughness element induces boundarylayer transition". *The Physics of Fluids*, Vol. 15, p. 1173–1178.

Masad, J.A. and Iyer, V., 1994. "Transition prediction and control in subsonic flow over a hump". *Physics of Fluids*, Vol. 6, No. 1, pp. 313–327.

Nayfeh, A.H., Ragab, S.A. and Al-Maaitah, A.A., 1988. "Effect of bulges on the stability of boundary layers". *The Physics of Fluids*, Vol. 31, No. 4, pp. 796–806.

Reneaux, J., 2004. "Overview on drag reduction technologies for civil transport aircraft". *European Congress on Computational Methods in Applied Sciences and Engineering (ECCOMAS)*, pp. 1–18.

Rossiter, J.E., 1966. "Wind-tunnel experiments on the flow over rectangular cavities at subsonic and transonic speeds". Technical Report R M No. 3438, Aeronautical Research Council.

Saric, W.S., Reed, H.L. and Kerschen, E.J., 2002. "Boundary-layer receptivity to freestream disturbances". *Annual Review of Fluid Mechanics*, Vol. 34, No. 1, pp. 291–319.

Sarohia, V., 1977. "Experimental investigation of oscillations in flows over shallow cavities". *AIAA JOURNAL*, Vol. 15, pp. 984–991.

Schubauer, G.B. and Skramstad, H.K., 1947. "Laminar boundary-layer oscillations and stability of laminar flow". *JOURNAL OF THE AERONAUTICAL SCIENCES*, Vol. 14, p. 69–78.

Sinha, S.N., Gupta, A.K. and Oberai, M.M., 1982. "Laminar separating flow over backsteps and cavities part ii: Cavities". *AIAA JOURNAL*, Vol. 20, pp. 370–375.

Smith, A., Company, D.A., Gamberoni, N., Sub-Committee, A.R.C.F.M. and Department, D.A.C.E.S.D.E., 1956. *Transition, Pressure Gradient and Stability Theory*. Douglas Aircraft Company, El Segundo Division.

Stuper, J., 1949. "The influence of surface irregularities on transition with various pressure gradients,". *Division of Aeronautics, Australia,*, Vol. 9.

Tani, I., Hama, R. and Mituisi, S., 1940. "On the permissible roughness in the laminar boundary layer,". *JAero. Res. Inst. Tokyo*.

van Ingen, J., 1956. "A suggested semi-empirical method for the calculation of the boundary layer transition region".

Victorino, V.B., Aguirre, F.O. and de Medeiros, M.A.F., 2023. "Gap induced boundary layer transition". *AIAA AVIATION Forum*, pp. 1–14.

Wang, Y.X. and Gaster, M., 2005. "Effect of surface steps on boundary layer transition". *Experiments in Fluids*, Vol. 39, p. 679–686.

7. RESPONSIBILITY NOTICE

The authors are solely responsible for the printed material included in this paper.